Available online at www.mjesci .com
AL-MUTHANNA JOURNAL FOR ENGENERING SCIENCES
مجلة المثنى للعلوم الهندسية

THE EFFECT OF ENTRANCE REGION GEOMETRY ON SOLAR CHIMNEY POWER PLANT PERFORMANCE.

Arkan Kh. Al-Taie [a], Ali Hayder Mutib[b]
[a] Machines and Equipment Engineering Department, University of Technology/Baghdad.
[b] Machines and Equipment Engineering Department, University of Technology/Baghdad.

ARTICLE INFO

Received: 26/5/2014

Accepted:30/11/2014

Keywords
Solar chimney, Numerical simulation , Junction type, Performance parameters.

ABSTRACT

A numerical simulation to investigate the performance of solar chimney power plant is presented**.** A small scale model of solar chimney power plant was modelled by using FLUENT software. The solar chimney power plants consist of three essential elements, glass roof collector, chimney (tower) and wind turbine. The output power of the system depends on the input velocity to wind turbine. The turbine inlet velocity is a function of collector – chimney junction type. To solve the governing equations of conservation of mass, momentum, energy, Do- intensity, k and ϵ equations the finite volume method was adopted by FLUENT software to model and analyze such system. The results showed that the geometry of entrance region (collector-chimney junction type) has an effect on the performance parameters especially air flow velocity. Using curved or rounded junction with deflector will improve system mass flow rate by 37.65% as compared with straight junction.

تأثير الشكل الهندسي لمنطقة المدخل على اداء المدخنة محطة الطاقة الشمسية.

الكلمات المفتاحية
المدخنة الشمسية ،محاكاة نظرية، توصيلة الارتباط، معاملات الاداء.

الخلاصة

في هذا البحث تم اجراء دراسة نظرية للتحقق من اداء محطة طاقة المدخنة الشمسية. نموذج مصغر من محطة طاقة المدخنة الشمسية تمت نمذجته باستخدام برنامج FLUENT. محطات طاقة المدخنة الشمسية تتكون من ثلاثة مكونات اساسية، مجمع شمسي ذو سقف زجاجي، المدخنة (البرج) و التوربين الهوائي. القدرة الخارجية للنظام تعتمد على السرعة الداخلة للتوربين الهوائي. السرعة الداخلة للتوربين هي دالة لنوع وصلة الارتباط بين المجمع الشمسي والمدخنة. لحل المعادلات الحاكمة مثل معادلات حفظ الكتلة ،الزخم ، الطاقة ،Do-intensity ، K و ϵ طريقة الحجوم المحددة اعتمدت بواسطة برنامج FLUENT لنمذجة وتحليل مثل هذه الانظمة. النتائج بينت ان الشكل الهندسي لمنطقة الدخول (نوع توصيلة الارتباط بين المجمع الشمسي والمدخنة) لها تأثير على معاملات الاداء وخصوصاً على سرعة تدفق الهواء. استخدام الوصلات المنحنية او المدورة مع الموجه سيحسن من التدفق الكتلي بنسبة 38% مقارنة بالوصلة المستقيمة.

E-mail addresses: arkanaltaie@yahoo.com[a], ahmiceng1990@yahoo.com[b]

DOI:10.52113/3/eng/mjet/2015-03-02/17-31

Introduction

A solar chimney power plant is a technology that uses solar energy to produce an artificial wind to generate electricity. Solar chimney power plants consist of three essential elements, circular glass roof solar collector (Air heating device), chimney or Tower (Power Generating Component) and wind turbine [1]. Air enters the collector from its periphery and is heated under the collector by heat emitted from glass roof and absorbing plate. It moves with a radial direction forward toward collector center where chimney base is. The temperature differential between the cool air at the top and the heated air at the bottom creates what is known as "the chimney effect or stack effect" results in a buoyancy force that drives the flow upward and out of the tower. A turbine installed at the base of the tower (for easier access and maintenance) used to extract the available power of flow and converting it to mechanical power (shaft work). Finally, a generator attached to the turbine provides electrical power [2]. Fig (1) shows a schematic layout of solar chimney power plant which illustrates the principle of operation**.**The geometric parameters of chimney height, collector and base area were investigated by Ali K. Al-Abadi [3].The influence of quality collector roof glass and various types of soil on the performance of a large scale solar chimney power plant were studied by J.P. Pretorius et al.,[4]. By using numerical analysis based on the (Finite Difference Technique) H. H. Al-Kayiem et al.,[5] studied effects of geometries variations (collector covers orientation and the chimney configuration) on the performance of the system. E. BACHAROUDIS et al.,[6] use the control volume method to solve the governing elliptic equations for two-dimensional domain to investigate the thermo fluid phenomena occurring inside solar chimneys. Sh. Khoshmanesh [7] used FLUENT software to study the variation of velocity with five parameters of the systems which is Absorber Diameter (D_p), Roof glass angle (β), Entrance height (h), Tower's Height (h_t) and Tower's Diameter (D_t). Atit Koonsrisuk et al.,[8] used computational fluid dynamic technology (CFD) to investigate the changes in flow kinetic energy caused by the variation of tower flow area with height. The geometry of the major components of the Solar Chimney Power Plant, (solar air collector, chimney tower, and wind turbine) were studied and optimized by Sandeep K. Patel et al.,[9].

The present study investigates the influence of **"**collector – chimney junction type**"** on the performance parameters of solar chimney power plant. Four types of solar chimney power plant were modelled and simulated. Each one differs in junction type. Which are straight, curved (r = 0.025), curved (r = 0.05) junction and curved junction with deflector, as shown in Figures (2-A to 2D)

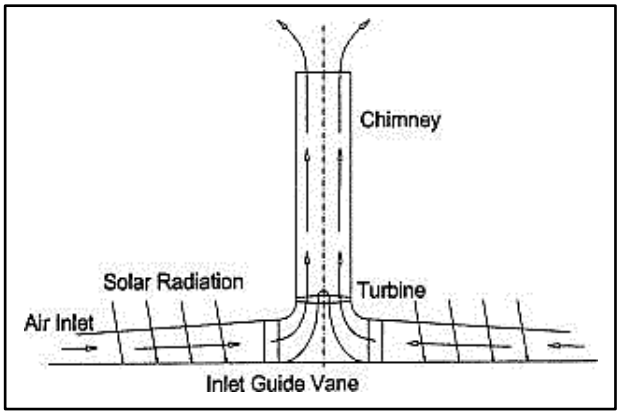

Figure 1. schematic layout of solar chimney power plant.

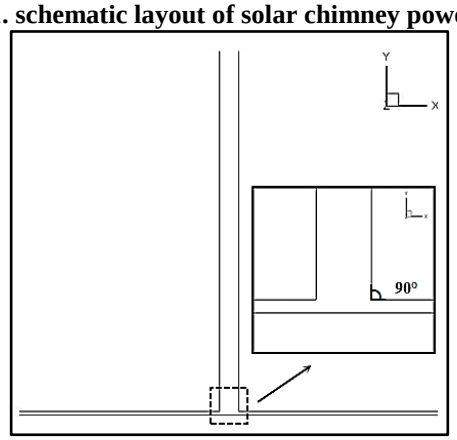

Figure (2-A): Schematic layout shows straight junction type.

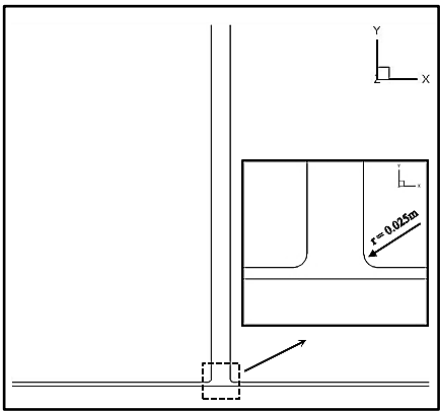

Figure (2-B): Schematic layout shows curved junction (r = 0.025m).

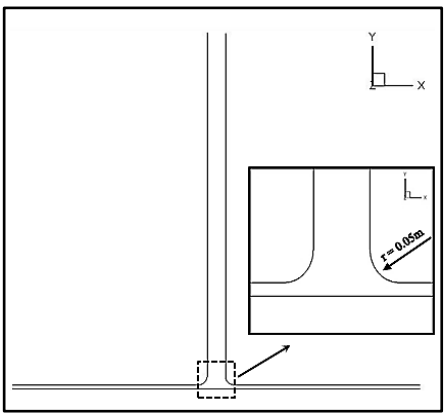

Figure (2-C): Schematic layout shows curved junction (r = 0.05m).

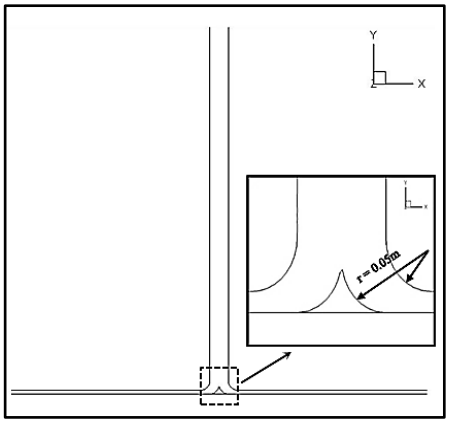

Figure (2-D): Schematic layout shows curved junction (r = 0.05m) with deflector.

Numerical simulation.

Physical model

The Manzanares pilot plant 1:100 scaled model was selected as the physical model to verify the numerical method. The computational domain is divided into the following zones: the collector, absorbing plate, chimney, and airflow. Figure (3) shows the power plant scale model and its dimensions.

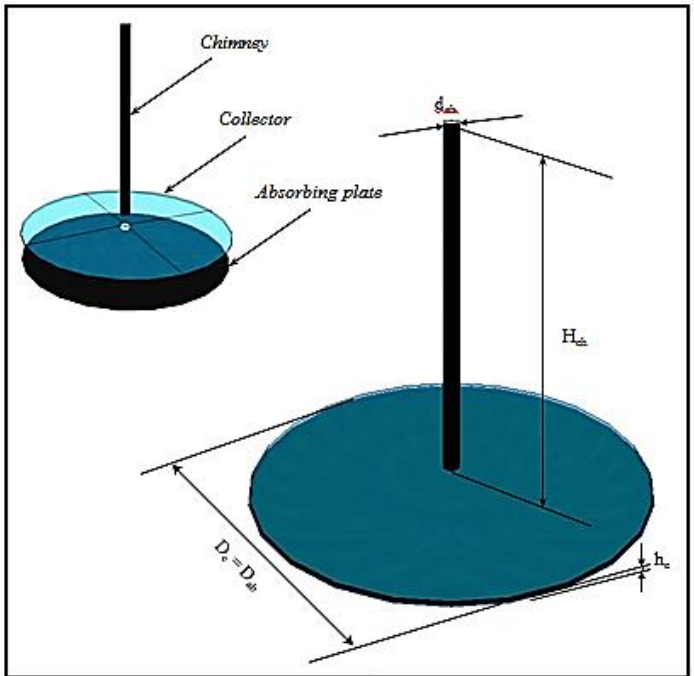

Chimney height (H_{ch})	1.95 m
Collector gap (h_c)	0.019m
Chimney diameter (d_{ch})	0.1m
Collector diameter (D_c)	2.24 m
Absorbing plate diameter (D_{ab})	2.24 m

Figure (3): power plant scale model and its dimensions.

Mesh Generation

GAMBIT 2.2.30 software was used for grid generation. The computational domain was discretized using the Triangular/ tetrahedral meshes. The Tetrahedral grid used ensures that the results obtained are of the highest quality and accuracy. Meshing for solar chimney with straight and curved junction are shown in Fig. (4). A grid independence test was done using three different grid sizes of 805,624, 2,306,534and 2,684,867 nodes respectively. The judging criterion was the mass flow rate. The mass flow rates obtained were 0.0047, 0.01381and 0.01365 kg/s. The mass flow rate obtained at 2,306,534 and 2,684,867 nodes grid size showed very little difference which was of the order of 1.15%. So having a very fine mesh would not have been beneficial as it would have prolonged the simulation time and for this reason, a grid size of 2,306,534 nodes was chosen for all the simulations.

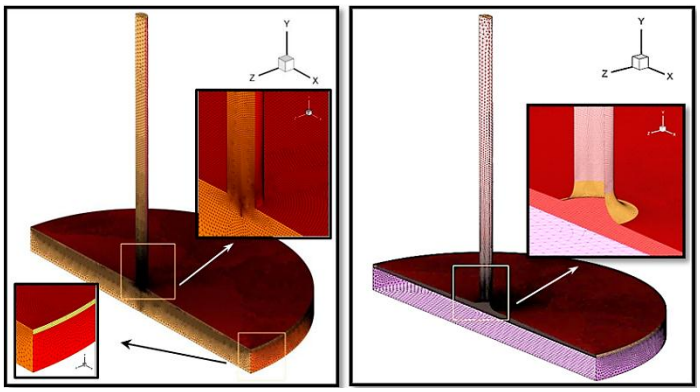

Figure (4): Meshing of straight and curved junction solar chimney physical model.

Assumptions.

In the present study, the flow characteristics are assumed to be as follows,

1. Steady flow.
2. Three dimensional.
3. The working fluid is air and behaves as an ideal gas.
4. Incompressible fluid.
5. Turbulent flow.
6. Newtonian fluid.

Modeling.

All simulations in this study was carried out using the finite volume-based solver FLUENT 6.3.26. Steady state analysis was chosen. The working fluid used was air which was modelled as an ideal gas. The entire model was built from the origin and extended in the positive y-direction. The buoyancy model was activated by specifying the gravity of -9.81m/s^2 in the y-direction which represented real life flow. The reference pressure used was101325 Pascal. Heat transfer in the solar chimney power plant system involves all three modes: conduction, convection, and radiation. In simulating the flow in solar chimney power plant, computations using models that only focus on conduction or convection are the simplest, whereas those involving buoyancy-driven flow and radiation models are more complex. Radiation heat transfer mainly occurs in the collector, which is covered by different types of semi-transparent materials such as glass or plastic. The cover materials are nearly transparent for incident solar radiation but partly opaque for infrared radiation from the ground. In the present simulations, the discrete ordinate (DO) radiation model was adopted to solve the radiative transfer equation for the following reasons: (1) only the DO model can be used to model semi-transparent walls of various types, (2) only the DO model can be used to compute non-gray radiation using a gray band model, (3) the DO model can work well across a full range of

optical thicknesses, (4) Computational cost is moderate for typical angular discretization and (5) memory requirements are modest. The (DO) Irradiation model used to applying a solar load directly to the DO model (the irradiation flux is applied directly to semi-transparent walls) that specified as a boundary condition, and the radiative heat transfer is derived from the solution of the DO radiative transfer equation. Solar radiation is modelled using the sun's position vector and illumination parameters, which can be specified by users or by a solar calculator utility provided by FLUENT. Solar load is available for 3-D simulation only and can be used to model steady and unsteady flows. Flow in solar chimney power plant is a kind of buoyancy-driven flow. The strength of the buoyancy-induced flow is measured by the Rayleigh number. Rayleigh number less than 10^7 indicate a buoyancy-induced laminar flow, with transition to turbulence occurring over the range of $10^7 <$ Ra $< 10^{11}$. The Rayleigh number for solar chimney scale model is greater than 10^8 that indicate a buoyancy-induced turbulent flow. Therefore, the k-ϵ turbulence model was selected to describe the airflow inside the system. The Boussinesq model was adopted in this simulation. This model treats density as a constant value in all solved equations, except for the buoyancy term in the momentum equation.

$$(\rho - \rho_\infty)g \approx - \rho_\infty \beta (T - T_\infty)g$$

Faster convergence can be achieved by using the Boussinesq model than by setting air density as a function of temperature. The basic equations that describe the movement of the flow are:-

Conservation of Mass (Continuity).

$$\frac{\partial u}{\partial x} + \frac{\partial v}{\partial y} + \frac{\partial w}{\partial z} = 0 \quad \text{..... (1)}$$

Navier-Stokes Equations (Momentum).

$$\frac{\partial(\rho uu)}{\partial x} + \frac{\partial(\rho vu)}{\partial y} + \frac{\partial(\rho wu)}{\partial z} = -\frac{\partial p}{\partial x} + \mu\left[\frac{\partial^2 u}{\partial x^2} + \frac{\partial^2 u}{\partial y^2} + \frac{\partial^2 u}{\partial z^2}\right] \quad \text{.....} \quad (2)$$

$$\frac{\partial(\rho uv)}{\partial x} + \frac{\partial(\rho vv)}{\partial y} + \frac{\partial(\rho wv)}{\partial z} = -\frac{\partial p}{\partial y} + \mu\left[\frac{\partial^2 v}{\partial x^2} + \frac{\partial^2 v}{\partial y^2} + \frac{\partial^2 v}{\partial z^2}\right] + S_{bj} \quad \text{...(3)}$$

$$\frac{\partial(\rho uw)}{\partial x} + \frac{\partial(\rho vw)}{\partial y} + \frac{\partial(\rho ww)}{\partial z} = -\frac{\partial p}{\partial z} + \mu\left[\frac{\partial^2 w}{\partial x^2} + \frac{\partial^2 w}{\partial y^2} + \frac{\partial^2 w}{\partial z^2}\right] \text{.....} \quad (4)$$

Energy Equation.

$$\rho\frac{\partial}{\partial x}(uT) + \rho\frac{\partial}{\partial y}(vT) + \rho\frac{\partial}{\partial z}(wT) = \frac{\partial}{\partial x}\left(\Gamma_{eff.h}\frac{\partial T}{\partial x}\right) + \frac{\partial}{\partial y}\left(\Gamma_{eff.h}\frac{\partial T}{\partial y}\right) + \frac{\partial}{\partial z}\left(\Gamma_{eff.h}\frac{\partial T}{\partial z}\right) + S_T \quad \text{.....(5)}$$

k-ϵ Equations.

Turbulence kinetic energy (k) equation:-

$$\frac{\partial}{\partial x_i}(\rho k u_i) = \frac{\partial}{\partial x_j}\left[\left(\mu + \frac{\mu_t}{\sigma_k}\right)\frac{\partial k}{\partial X_j}\right] + G_K + G_b - \rho\epsilon + S_k \quad \text{.....(6)}$$

The dissipation rate of turbulence energy (ϵ) equation:-

$$\frac{\partial}{\partial x_i}(\rho\epsilon u_i) = \frac{\partial}{\partial x_j}\left[\left(\mu + \frac{\mu_t}{\sigma_\epsilon}\right)\frac{\partial \epsilon}{\partial X_j}\right] + C_{1\epsilon}\frac{\epsilon}{k}(G_k + C_{3\epsilon}G_b) - C_{2\epsilon}\rho\frac{\epsilon^2}{k} + S_\epsilon \quad \text{..... (7)}$$

Where.

$$G_k = -\rho\overline{u_i' u_j'}\frac{\partial u_j}{\partial x_i} \; ; \qquad G_b = \beta g_i \frac{\mu_t}{Pr_t}\frac{\partial T}{\partial x_i}$$

($C_{1\epsilon}, C_{2\epsilon}, C_\mu, \sigma_k and\ \sigma_\epsilon$) are the model constants and have default values illustrated in Table (1).

Table (1): The k − ϵ Turbulence Model Constants.

$C_{1\epsilon}$	$C_{2\epsilon}$	C_μ	σ_K	σ_E
1.44	1.92	0.09	1	1.3

Do-intensity equation.

$$\nabla.(I(\vec{r},\vec{s})\vec{s}) + (\alpha + \sigma_s)I(\vec{r},\vec{s}) = \alpha n^2\frac{\sigma T^4}{\pi} + \frac{\sigma_s}{4\pi}\int_0^{4\pi} I(\vec{r},\vec{s}')\Phi(\vec{s}.\vec{s}')\,d\Omega' \text{....(8)}$$

Boundary conditions.

Boundary conditions specify the flow and thermal variables on the boundaries of the physical model. The boundary conditions applied in this present work are those shown in Fig. (5) and Table (2). Tables (3) and (4) show the momentum and turbulence boundary conditions for the whole parameters of the Solar Chimney Power Plant model in details. Tables (5) and (6) show the radiation boundary conditions and thermal condition in details.

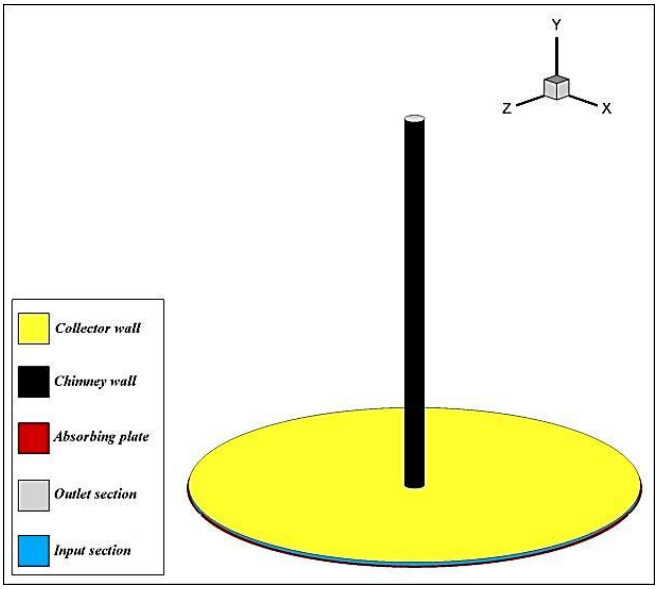

Figure (5): Boundary conditions of the solar chimney model.

Table (2): Boundary Conditions Types of solar chimney model.

Zone	Type
Chimney	Wall
Collector	Wall
Absorbing plate	Wall
Inlet section	Pressure inlet
Outlet section	Pressure outlet
Air	Fluid

Table (3): Momentum boundary condition

Part	Type	Momentum Conditions
Input section	Pressure inlet	- Gauge pressure = (0 Pascal), [constant].
		- Turbulent Intensity = 10%
		- Hydraulic diameter = 0.038m
Outlet section	Pressure outlet	- Gauge pressure = (0 Pascal), [constant].
		- Turbulent Intensity = 10%
		- Hydraulic diameter = 0.1

Part	Type	Momentum Conditions	
		Wall Motion	Shear Condition
Chimney	Wall	Stationary	No Slipping
Collector	Wall	Stationary	No Slipping
Absorbing plate	Wall	Stationary	No Slipping
Input section	Pressure inlet	- Gauge Pressure = (0 Pascal), [constant]. - Flow direction specification Method : (Normal to Boundary).	
Outlet section	Pressure Outlet	- Gauge Pressure = (0 Pascal), [constant]. - Backflow Direction specification Method: (Normal to Boundary).	

Table (4): Thermal boundary conditions..

Part	Type	Thermal Conditions
Chimney	Mixed	-Heat transfer coefficient = 8.29 W/m2-K - Free stream temperature = $\mathbf{T}_\infty$ = 46 °C - External emissivity = 0.86 - External radiation Temperature = 0.0552 $\mathbf{T}_\infty^{\mathbf{1.5}}$ - Wall Thickness = 0.003 m. - Heat generation Rate = 0 (W/m3).
Collector	Mixed	-Heat transfer coefficient = 8.29 W/m2-K - Free stream temperature = $\mathbf{T}_\infty$ = 46 °C - External emissivity = 0.87 - External radiation temperature = 0.0552 $\mathbf{T}_\infty^{\mathbf{1.5}}$ - Wall Thickness = 0.004 m. - Heat generation Rate = 0 (W/m3).
Upper tank wall (Absorber plate)	Coupled	- Wall Thickness = 0.0015 (m). - Heat generation Rate = 0 (W/m^3).
Input section	Pressure inlet	-Total temperature = 46 °C
Outlet section	Pressure outlet	-Backflow Total Temperature = 46 °C

Table (5): Radiation boundary conditions.

Part	Radiation Boundary Conditions
Chimney	Opaque or Semi-transparent
Collector	Semi-transparent (I = 807.56 W/m^2)
Absorber plate	Opaque
Input section	External black body temperature = Boundary temperature
Outlet section	External black body temperature = Boundary temperature

Solution method.

The governing equations are solved on a staggered grid and the coupling between the momentum and continuity equations through pressure is based on the simple (Semi Implicit Pressure Linked Equation) scheme. The second order, upwind scheme is applied for convective terms of the momentum and energy transport equations, whereas pressure is discretised using the PRESTO! (PREssure STaggering Option) scheme. To ensure numerical stability, the discretized equations are solved by iteration with under-relaxation factors of 0.3 for pressure, 0.7 for momentum, and 0.8 for turbulent kinetic energy, turbulent dissipation rate and 1 for density, body force, turbulent viscosity, Do-Intensity and energy. Solution convergence is controlled by setting the convergence criterion (residual) to 10^{-3} for each equation except for the energy and Do-Intensity equations, which is set to 10^{-6}. All results reported in this paper are obtained using a double precision solver.

Calculations.

1- *Air mass flow rate* can be calculate as follow:-

$$\dot{m}_a = \rho_a \, . V_a \, . A_{ch} \quad \text{.....} \quad (9)$$

2- *Available power* can be calculate as follow:-

$$P_{available} = 0.5 \, \rho_a \, . A_{ch} . V_a^3 \text{.....} \quad (10)$$

Results and discussion.

To show the effect of entrance geometry type junction on the performance of solar chimney power plant, the results of 4 tests are presented graphically in a form of performance curves from to predict the performance of plant. The FLUENT data results for four tests are shows in Fig. (11) to (13).

Performance Parameters.

1- Airflow Temperature.

The amount of air temperature rise through the collector indicates the amount of thermal energy gained by air stream, when it is flowing over the absorbing hot plate of the collector. Figure (6) shows the relation between air flow temperature and non-dimensional flow path from collector inlet to chimney outlet. It consists of four curves. Each curve shows that, the airflow temperature increases along the flow path in collector region and then abrupt dip and rise near chimney base, then decreased slowly along the flow path in chimney region. This is because that, the increasing of airflow temperature in collector region is caused by Greenhouse effect and heat transfer from absorbing hot plate. The abrupt dip and rise near chimney base is caused by the response of abrupt velocity change due to flow area reduction. The decreasing of airflow temperature along chimney region is caused by heat transfer from flowing hot air to the chimney wall.

As can be seen in this Figure, straight junction has highest airflow temperature distribution curve than curved or rounded junction with deflector. And the other two cases are at mid them. This is because of, the difference of velocity. Where, as velocity increase the air mass flow rate increases. That causes more air flow that picks a large amount of energy when it enter to the collector and out from the chimney.

2- Absorbing Plate Temperature.

The absorbing plate is heated up by solar radiation that comes from the sun and transmitted through the collector's glass. Figure (7) shows the relation between absorbing plate temperature and non-dimensional plate path from plate circumference to plate center. It shows that straight junction has highest absorbing plate temperature distribution than rounded junction with deflector and the other two cases mid them. This is because of difference of velocity, where, as velocity increases the air mass flow rate increases. That causes more air flow to pick a large amount of energy when it enters to the collector and out from it.

3- Airflow Velocity.

The motive force that move the flow from collector inlet gap to chimney outlet is caused by combined effect of the flow area reduction and amount of heat transfer from the absorbing plate along the film to the working fluid (air). Figure (8) shows the relation between airflow velocity and non-dimensional flow path from collector inlet to chimney outlet. It consist of four curves. Each curve shows that the airflow velocity increases gradually along the flow path in the collector region and then increases sharply near chimney base. After that, along the flow path in chimney region the velocity is tend to be stable and then increases slowly near chimney outlet section. This because that the increases of velocity in collector region is caused by the amount of heat transfer from the absorber plate along the film to the working fluid. This will increase the kinetic energy of air particles along the collector passage. The sharp increase of air flow velocity near solar collector center is caused by effect of flow area reduction. The airflow velocity is inversely proportional with solar collector radius because the solar collector design of the system has airflow direction to the center of the solar collector where chimney inlet section is (i.e.), if the air flow velocity at inlet to the solar collector from circumference (R_c) outer =1.12 m) has minimum value, inversely at the center of the solar collector where chimney is (Rc) inner = 0.05m) the airflow velocity has maximum value ($V_r \propto 1/R_c$). This agrees with [10]. The cause of stability of airflow velocity at mid chimney part caused by that the flow is fully developed (i.e.) when the flow enter the chimney a nearly inviscid upstream flow converges, viscous boundary layer grow downstream retarding the axial flow u(r, y) at the wall and thereby accelerating the center-core flow to maintain the incompressible continuity requirement. At a finite distance from the entrance the boundary layers merge and the inviscid core disappears, the flow is then entirely viscous, the axial velocity adjusts slightly further until at x = Le (entrance length) it no longer changes with x). The small increasing of airflow velocity in chimney region near the outlet section caused by amount of air temperature rise (ΔT) between ambient and chimney outlet. The chimney's outlet draft has a temperature higher than the ambient temperature, as it is known the density is inversely preoperational with temperature ($\rho \propto 1/T$). That indicates its density is lower than ambient, this will accelerate the flow. As can be seen in this Figure, rounded junction with deflector has highest airflow velocity distribution curve than straight junction and the other two cases mid them, while near the chimney inlet section the airflow velocity of straight junction suffers a sudden decline as compared with the other junction types. This because minor losses due to entrance geometry. At a straight junction the minor losses will be high due to what is known as "vena contracta phenomenon". According to this phenomenon the flow velocity increases sharply at entrance region with abrupt dip in pressure because of flow separation and recirculation occurrence at dead air region near the straight junction in chimney wall entrance region. So, using curved or rounded junction will avoid this phenomenon and improve the flow velocity. The deflector is used to direct the flow along the passage from collector to the chimney and avoid the flow recirculation occurrence at collector center under chimney inlet section all that leads to improve velocity of flow.

4- Working Air Mass Flow Rate ($\dot{m}$).

Figure (9) shows the relation between working air mass flow rate Vs. average flow velocity at chimney inlet section. For four junction types. As can be seen from this figure, the working air mass flow rate increases linearly with increasing average flow velocity in each junction type, due to decreases in minor losses in chimney inlet section.

5- Flow Available Power ($P_{available}$).

It represents the flow kinetic energy when all pressure difference in the tower is converted to velocity in case of without turbine in the tower. Figure (10) shows the relation between flow available power Vs. air mass flow rate at chimney inlet section. For four junction types. As can be seen from this Figure, the flow available power increases linearly with increasing air mass flow rate due to increase in average flow velocity at chimney inlet section in each junction type.

Conclusions.

The geometry of entrance region (collector-chimney junction type) has an effect on the performance parameters. the results showed that

1- Using curved or rounded junction instead of straight junction will minimize miner losses and keeps the velocity along chimney region.

2- Using curved or rounded junction with deflector will improve flow velocity by directing the flow toward chimney without circulation formation at collector center.

3- The best test was when using curved or rounded junction with deflector. This will improve system mass flow rate by 37.65% as compared with straight junction.

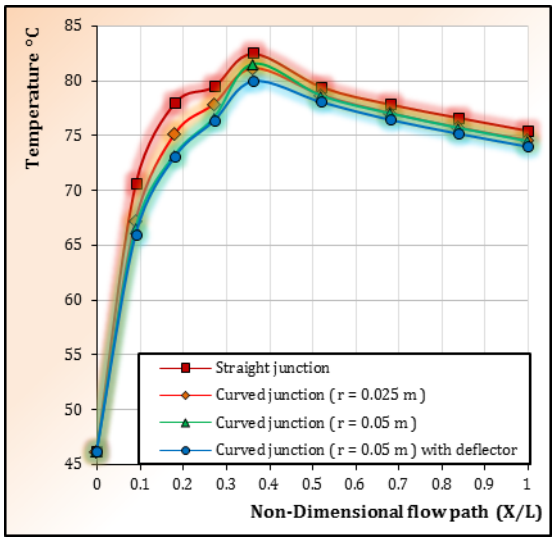

Figure (6): Air flow temperature distribution for fourth junction types.

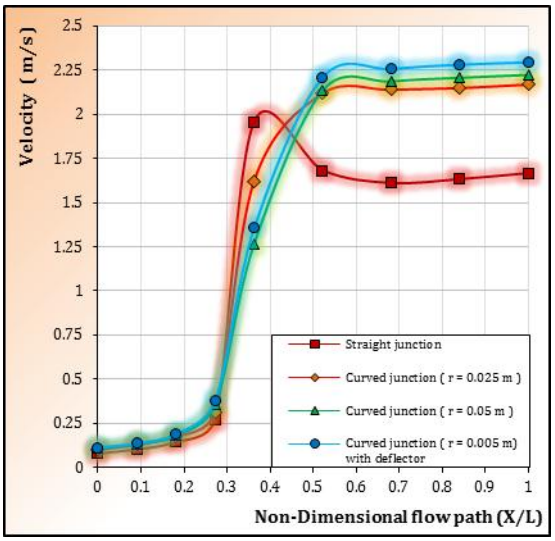

Figure (8): Airflow velocity distribution of fourth junction types.

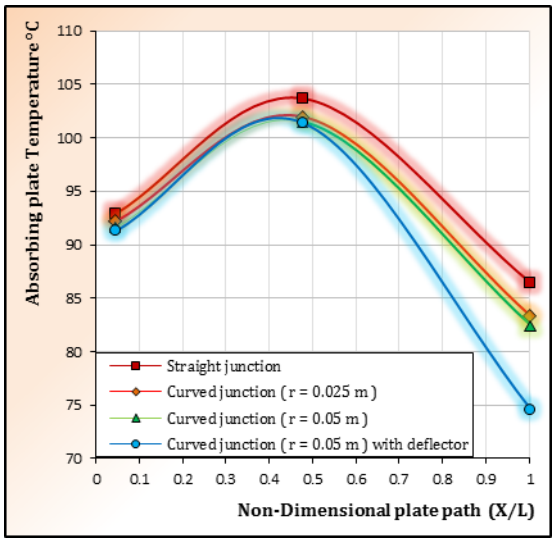

Figure (7): Absorber plate temperature distribution for fourth junction types.

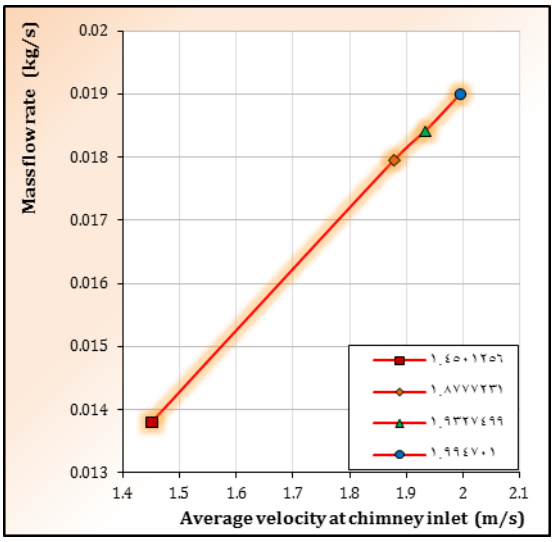

Figure (9): Working air mass flow rate Vs. average velocity of fourth junction types.

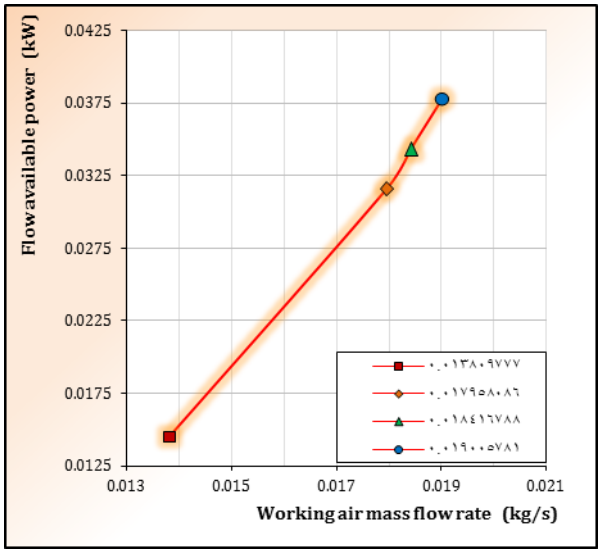

Figure (10): Flow available power Vs. Working air mass flow rate of fourth junction types.

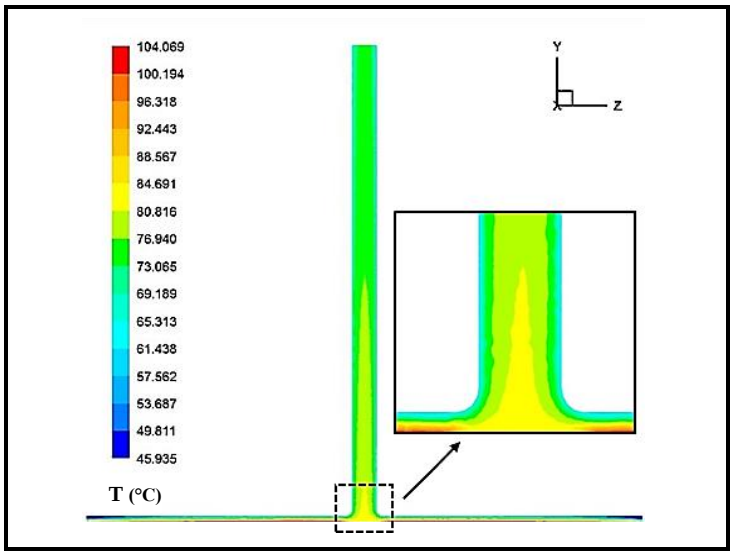

Figure (11-B): Longitudinal section of temperature contour for curved junction (r = 0.025m) type.

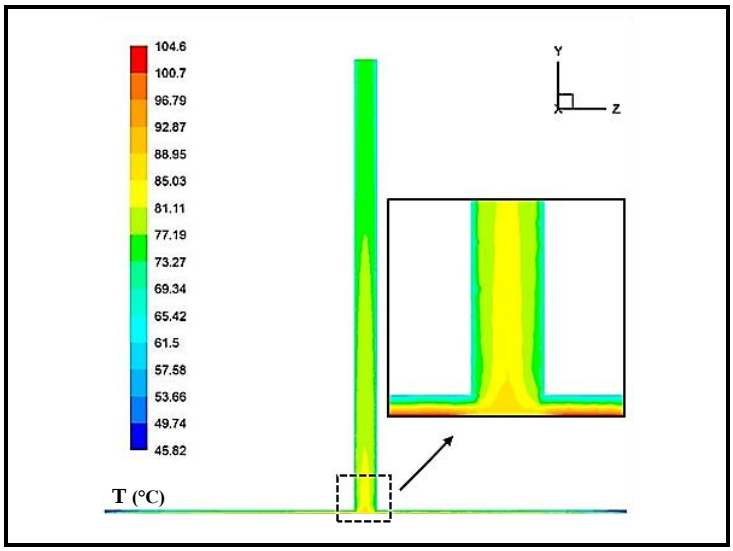

Figure (11-A): Longitudinal section of temperature contour for straight junction type.

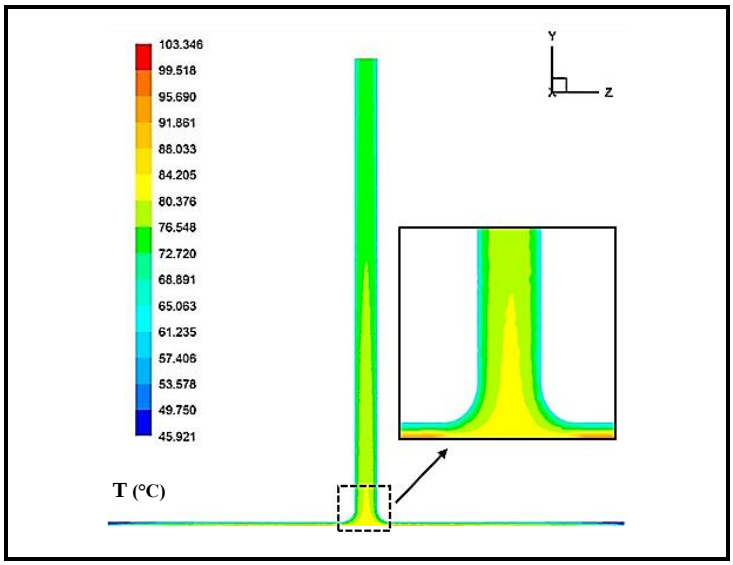

Figure (11-C): Longitudinal section of temperature contour for curved junction (r = 0.05m) type.

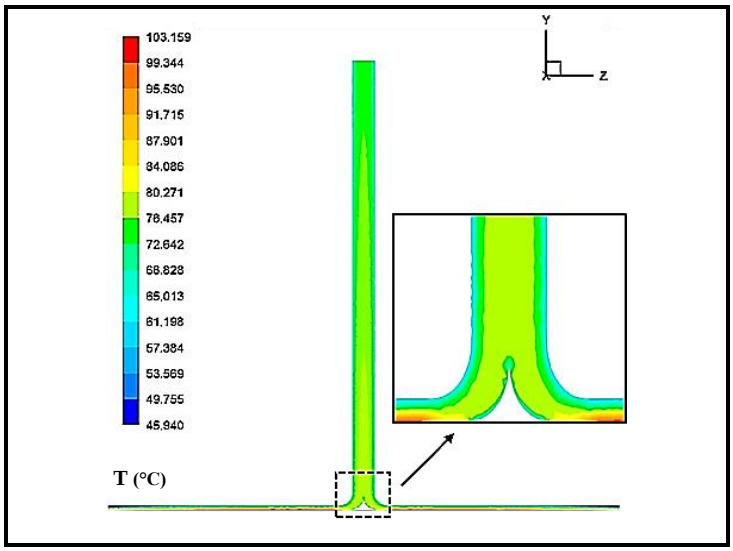

Figure (11-D): Longitudinal section of temperature contour for curved junction (r = 0.05m) with deflector.

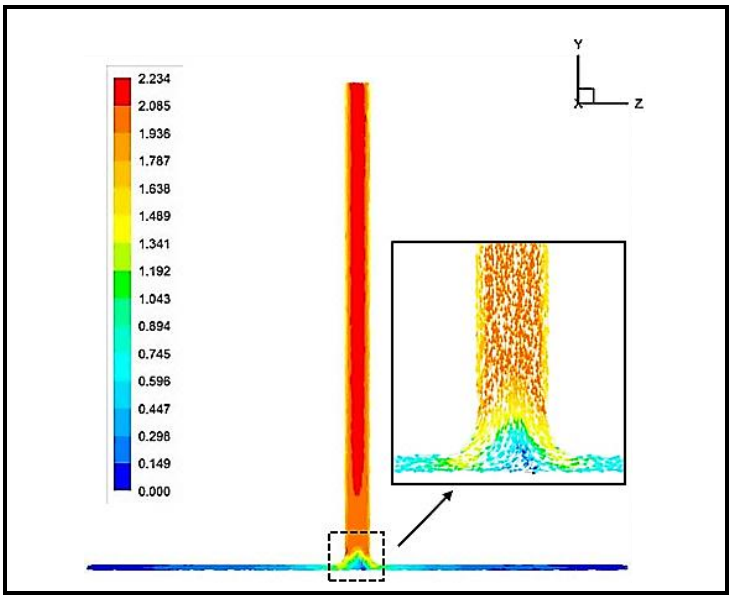

Figure (12-C): Longitudinal section of velocity vector contour for curved junction (r = 0.05m) type.

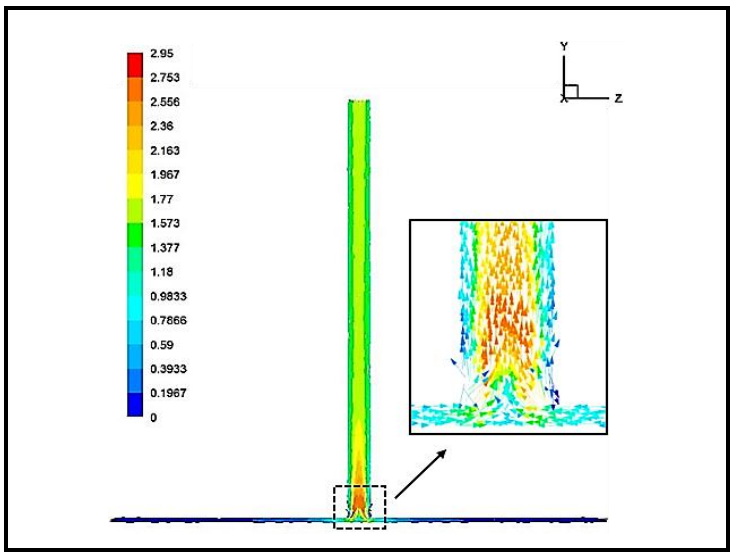

Figure (12-A): Longitudinal section of velocity vector contour for straight junction type.

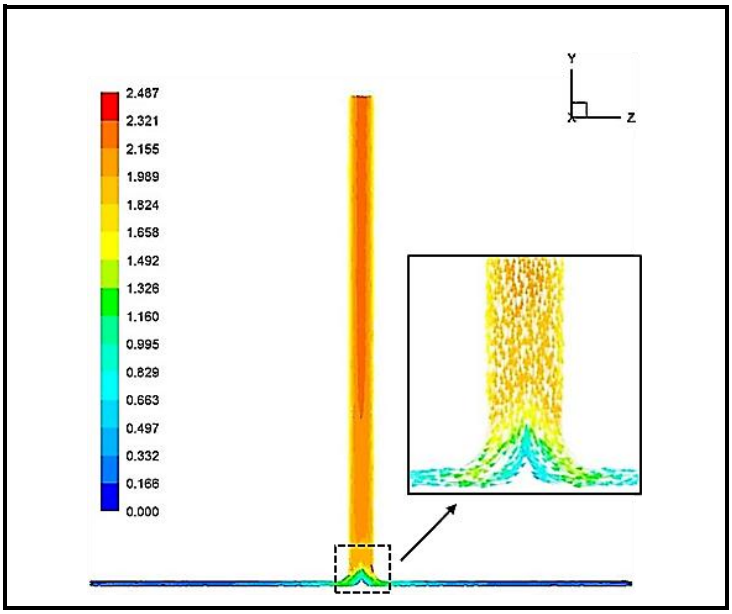

Figure (12-D): Longitudinal section of velocity vector contour for curved junction (r = 0.05m) with deflector

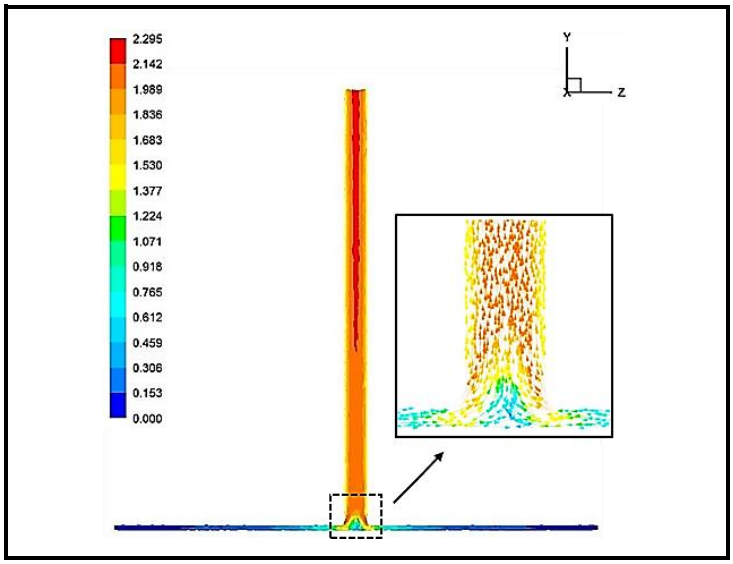

Figure (12-B): Longitudinal section of velocity vector contour for curved junction (r = 0.025m) type.

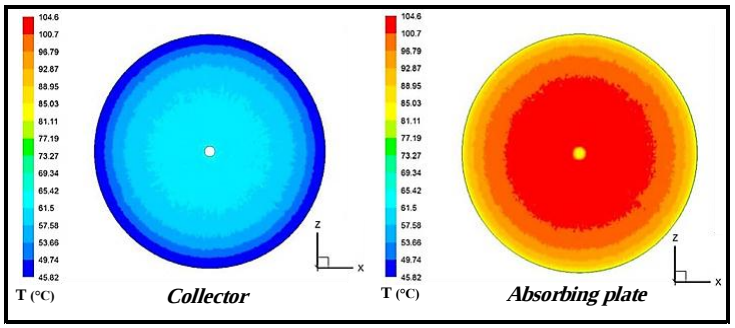

Figure (13-A): Cross-section of temperature contour for straight junction type.

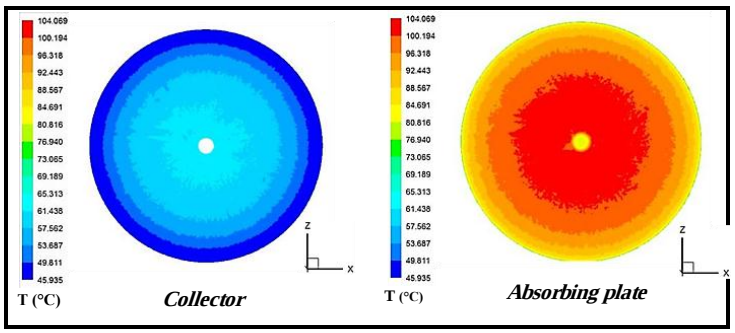

Figure (13-B): Cross-section of temperature contour for curved junction (r = 0.025m) type.

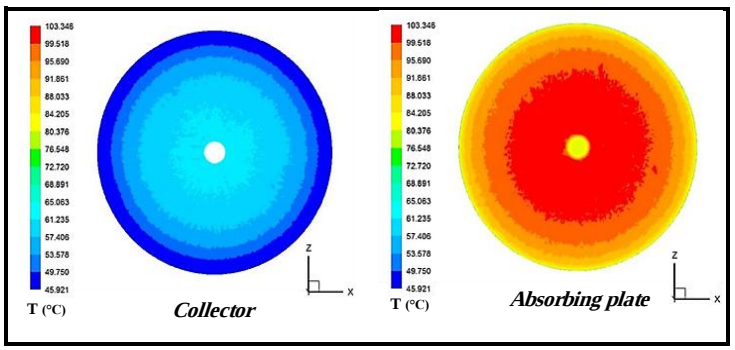

Figure (13-C): Cross-section of temperature contour for curved junction (r = 0.025m) with deflector.

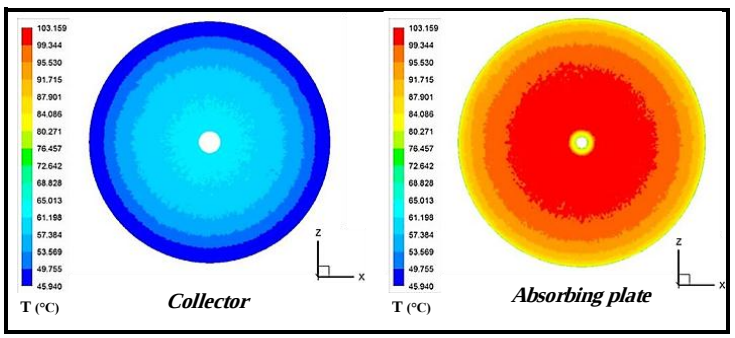

Figure (13-D): Cross-section of temperature contour for curved junction (r = 0.05m) with deflector.

Abbreviations	
Abbreviations	**Description**
CFD	*Computational Fluid Dynamics*
DO	*Discrete Ordinates*
FLUENT	*Fluid And Heat Transfer Code*
GAMBIT	*Geometry And Mesh Building Intelligent Toolkit*
PRESTO!	*Pressure Staggering Option*

Nomenclature		
Symbol	**Description**	**Unit**
A	Area	m^2
a	Absorption coefficient	---
$C_{1\varepsilon}$, $C_{2\varepsilon}$, $C_{3\varepsilon}$, C_μ	Turbulence Model Constants	---
g	Gravitational Acceleration (9.81)	m/s^2
G_b	Generation of turbulence kinetic energy due to buoyancy	---
G_k	Generation of turbulence kinetic energy due to the mean velocity gradients	---
I	Radiation intensity	W/m^2
k	Turbulence Kinetic energy	---
$\dot{\mathbf{m}}$	Mass Flow Rate	kg/s
n	Refractive index	---
P	Available Power	kW
$\vec{\mathbf{r}}$	Position vector	---
S_{bj}	Buoyancy source or sink term	---
$\vec{\mathbf{s}}$	Direction vector	---
$\vec{\mathbf{s}}'$	Scattering direction vector	---
$\mathbf{S_k}$, $\mathbf{S_\epsilon}$,$\mathbf{S_T}$	User-defined source terms	---
T	Temperature	^oC
u	Stream-wise velocity	m/s
v	Velocity	m/s
v	Lateral velocity	m/s
w	Vertical velocity	m/s
x, y, z	The corresponding Cartesian axis	---
Greek Symbols		
Symbol	**Description**	**Unit**
∂	Partial differential operator	---
β	Thermal expansion coefficient	1/K
ϵ	Turbulence energy dissipation rate	---
μ	Dynamic viscosity	Pa.m
ρ	Density	kg/m^3
σ_k , σ_ε	Turbulent Prandtl number for K and ε	---
$\boldsymbol{\sigma_s}$	Scattering coefficient	---
Φ	Phase function	---
Γ	Diffusion coefficient	---
Ω′	Solid angle	Degree

Subscripts	
Subscript	**Description**
av	Average
c	Collector
ch	Chimney
eff	Effective condition
i, j, k	The three coordinate directions
t	Turbulent flow condition, total
∞	Ambient

References

1.Jeffrey Freidberg, 2008, "Solar updraft towers: their role in remote on-site generation", pp 1-31.

2. Schlaich Bergermann und partner, 2002, "the solar chimney", Structural Consulting Engineers, pp 1-14.

3. Ali K. Al-Abadi, Ahmed F. Kridi and Ghassan Fadhil M. Hussain, 2010, "COMPARISON BETWEEN SIMULATED AND CALCULATED POWER OF THE SOLAR CHIMNEY WITH BLACK CONCRETE BASE USING ANSYS PROGRAM", Al-Qadisiya Journal For Engineering Sciences, Vol. 3, No. 3, pp. 347-364.

4.J.P. Pretorius and D.G. Kröger, 2005," Critical evaluation of solar chimney power plant performance", Science Direct, pp. 535-545.

5. H. H. Al-Kayiem and Q. A. Al-Nakeeb, 2006, " Geometry Alteration Effect on the Performance of a Solar-Wind Power System, International Conference on Energy & Environmental Systems(ICEE).

6.E. BACHAROUDIS, M.GR. VRACHOPOULOS, M.K. KOUKOU and A.E. FILIOS, 2006," Numerical investigation of the buoyancy-induced flow field and heat transfer inside solar chimneys", International Conference on Energy & Environmental Systems (ICEE), pp. 293-298.

7. Sh. Khoshmanesh, 2006, "Computer Simulation of Solar Updraft Tower Systems to Describe the Variation of Velocity with Essential Parameters of the Systems ", International Conference on Energy & Environmental Systems (ICEE), pp. 1-5.

8.Atit Koonsrisuk and Tawit Chitsomboon, 2006," Effect of Tower Area Change on the Potential of Solar Tower", Sustainable Energy and Environment (SEE), pp.1-6.

9. Sandeep K. Patel, Deepak Prasad and M. Rafiuddin Ahmed, 2014, "Computational studies on the effect of geometric parameters on the performance of a solar chimney power plant", Science Direct, pp. 424–431.

10. Hussam Abd-Alrazak Falih, 2004, " Design study of vertical solar chimney power plant", M.Sc. Thesis, Al-Nahrain University, Iraq.